Theor Chem Acc (2012) 131:1175
DOI 10.1007/s00214-012-1175-1

REGULAR ARTICLE

Probing O-dealkylation and deamination aging processes in tabun-conjugated AChE: a computational study

Manoj K. Kesharwani · Tusar Bandyopadhyay · Bishwajit Ganguly

Received: 19 April 2011 / Accepted: 14 January 2012 / Published online: 28 February 2012

Abstract The mechanisms of the aging process of tabun-conjugated acetylcholinesterase were explored using density functional theory calculations. The free energy surfaces were calculated for O-dealkylation (C–O bond breaking) and deamination (P–N bond breaking) pathways for the aging process of tabun-conjugated acetylcholinesterase as suggested by mass and crystallographic studies. Initially, the calculations were performed using tabun-conjugated serine (SUN) molecule. O-dealkylation mechanism proceeds via one-step S_N2 type process, whereas the deamination process proceeds via two steps addition–elimination reaction at the phosphorus center of SUN molecule. The recent proposal of another deamination mechanism using human butyrylcholinesterase (*h*BChE) conjugated with *N*-mono methyl analogue of tabun (TA4) has also been explored (Nachon et al. in Chem Biol Interact 187:44–48, 2010). The rate-determining activation barrier calculated for this deamination mechanism (26.3 kcal/mol) was comparable with O-dealkylation process (26.9 kcal/mol) with B3LYP/6-31+G* level of theory. To examine the influence of catalytic residue His447, additional calculations were performed with imidazole group of His447 residue. The incorporation of imidazole group of catalytic residue His447 showed marked decrease in the free energies of activation for all the studied aging processes of tabun-inhibited serine. The aging mechanisms have been explored with TA4-inhibited serine, and calculated results showed that the deamination with the rearrangement process is markedly preferred in this case, which supports the Nachon et al. proposal based on the crystallographic studies.

Keywords Aging process · Tabun · Acetylcholinesterase · Deamination · DFT calculations

1 Introduction

Acetylcholinesterase (AChE, EC 3.1.1.7) is one of the most important enzymes in many living organisms, including humans and vertebrates, and is located at the neuromuscular junction [1–3]. It is responsible for catalytic hydrolysis of neurotransmitter acetylcholine during nerve signal transmission [4–6]. Certain organophosphorus compounds (OPs) such as the nerve agents and a group of insecticides interfere with the catalytic mechanism of AChE by phosphylation (denotes phosphorylation, phosphonylation, and phosphoamidation) of serine hydroxyl group (Ser203 in *h*AChE), which is directly responsible for the hydrolysis of the neurotransmitter acetylcholine [2, 7–10]. Subsequent accumulation of acetylcholine at neuronal synapses and neuromuscular junctions results in various medical disorder such as paralysis, seizures, and other symptoms of cholinergic syndrome [11]. The OP-AChE conjugates can be treated with oxime-based medical antidotes, substances also known as reactivators, to restore the function of the inhibited enzyme [11–13]. This is an important step in the successful treatment of nerve agent poisoning, since it is

Electronic supplementary material The online version of this article (doi:10.1007/s00214-012-1175-1) contains supplementary material, which is available to authorized users.

M. K. Kesharwani · B. Ganguly (✉)
Analytical Science Discipline, Central Salt and Marine Chemicals Research Institute (Council of Scientific and Industrial Research), Bhavnagar, Gujarat 364 002, India
e-mail: ganguly@csmcri.org

T. Bandyopadhyay
Theoretical Chemistry Section, Chemistry Group, Bhabha Atomic Research Centre, Trombay, Mumbai 400 085, India

the only known practical means for recovering the activity of inhibited AChE. The efficacy of the oxime toward reactivation of OP-AChE conjugates depends on several factors such as the chemical structure of the oxime and OPs as well as the sequence of the AChE [14–18].

The phosphorus conjugate of the inhibited AChE may undergo a spontaneous, time-dependent elimination process, known as "aging", which usually involves dealkylation or deamination of the phosphorus conjugate. The dealkylation results in an oxyanion that forms a salt bridge with the protonated histidine [19, 20]. The salt bridge stabilizes the adduct and raises the energy barrier for the reactivation reaction, and leads to irreversibly inhibited enzyme. The aging process of AChE inhibited by sarin, soman, and VX yields a stable anionic methylphosphonylated (MeO_2P) reaction product, whereas two alternative pathways may be possible for phosphoroamidates (P–N agents) such as tabun. Also, the kinetics of the AChE inhibition and the aging of the conjugate depend on both the sequence of enzyme and the chemical structure of the conjugate. ChE inhibited by nerve agent soman undergoes the aging process within a few minutes [21], whereas ChE deactivated by tabun has an aging half-life of several hours [22].

Inhibition of AChEs by tabun and also the subsequent aging process are of particular interest due to the extraordinary resistance nature of tabun-AChE conjugates toward most oxime reactivators. The bimolecular rate constants with various oximes show that reactivation of tabun-*h*AChE has an intrinsically low reactivation rate than the more easily reactivated methylphosphonate [18, 23]. Interestingly, tabun-*h*AChE also exhibits a specific resistance toward reactivation by oxime HI-6 [18]. A crystallographic study of tabun-inhibited mouse AChE (*m*AChE) revealed a structural change in the side chains of His447 and Phe338, resulting in decreased active-site gorge dimensions. Based on this observation, it was suggested that the structural change of Phe338 may be one of the factors that contributes to the resistance toward reactivation by preventing bulky oximes to enter the catalytic site and access the phosphorus atom [24]. The crystal structure of HI6-*m*AChE also supports this hypothesis [25].

Aging mechanism of tabun-inhibited AChE is still not clear and is under debate. Mass spectrometry (MS) analysis of aged products of tabun-inhibited *h*AChE has suggested that the aging mechanism of tabun-AChE complex involved deamination of the phosphoramidate moiety [26, 27]. This was also supported by first crystallographic study of *m*AChE, but incomplete aging blurred the interpretation [24]. Later on, MS study of tabun-inhibited human butyrylcholinesterase (*h*BChE) showed that the loss of the dimethylamine substituent is rather an acid-catalyzed hydrolysis, which occurs during preparation of MS samples [28]. Crystallographic studies on tabun-inhibited *h*BChE and reinterpretation of previously reported *m*AChE data suggest the O-dealkylation of ethoxy group instead of deamination of dimethylamine during the aging of these ChEs [28].

According to proposed mechanism of O-dealkylation, the His447 imidazolium stabilizes a developing negative charge on the oxygen (C–$O^{\delta-}$ oxygen) of ethoxy substituent of tabun-ChE conjugates, and a water molecule activated by Glu202 attacks the newly appeared carbocationic center ($C^{\delta+}$–O carbon), leading to breaking of C–O bond and release of ethoxy group. The resulting negatively charged phosphoryl oxygen forms a salt bridge with the catalytic imidazolium residue [28]. The role of water in aging was initially suggested by Nachon et al. [29] with crystallographic study of echothiophate-inhibited *h*BChE. Recently, the X-ray crystal structure of aged tabun-*h*AChE complexed with fasciculin II also supports the dealkylation mechanism during the aging process [30]. However, in another work, it has been proposed that substitution-based aging also occurs for the *h*BChE adduct of an *N*-methyl tabun analogue (TA4, *N*-methyl-ethylphosphoramidofluoridate) and involves a rearrangement of the trigonal–bipyramidal transition state [31].

In this present article, we have explored the mechanism of the aging process of OPs-inhibited AChE employing quantum chemical calculations, which, however, was mainly reported on the basis of mass and crystallographic studies. The aging mechanisms of tabun-conjugated serine (SUN) involving deamination (P–N bond breaking) and O-dealkylation processes (C–O bond breaking) have been examined at DFT method. We have also examined another deamination process of aging, which involves a rearrangement of the trigonal–bipyramidal intermediate reported recently [31]. The role of catalytic residue His447 toward the aging process has also been investigated. Further, the aging process of tabun analogues TA4 is also examined in the light that the later one proceeds via deamination process involving the rearrangement mechanism.

2 Computational methodology

Tabun-conjugated serine (SUN) residue was modeled from reported PDB structure of tabun-conjugated acetylcholinesterase (PDB code: 2JEZ) [32]. The SUN was optimized at B3LYP/6-31+G* level in aqueous medium, prior to further use [33–36]. All calculations were performed with Gaussian 09 suite program [37]. Full geometry optimization of all stationary points was performed in aqueous phase at B3LYP/6-31+G* energy level with polarizable continuum solvation model (PCM) using the integral

equation formalism variant (IEF-PCM) [38–42]. The default UFF radii were used for the solvent calculations, which incorporate explicit hydrogen atoms [40]. In addition to this, full geometry optimization were also performed at B3LYP/6-31+G* energy level with SMD solvation model [43]. In SMD the "D" stands for "density" to denote that the full solute electron density is used without defining partial atomic charges [43]. We have reported the Gibbs free energy reaction profiles for the studied systems.

The stationary points were characterized by frequency calculations in order to verify that the transition structures had one, and only one, imaginary frequency. To verify that each saddle point connects two minima, intrinsic reaction coordinate (IRC) calculations of transition states were performed in both directions, that is, by following the eigenvectors associated to the unique negative eigenvalue of the Hessian matrix, using the González and Schlegel integration method [44, 45].

3 Results and discussion

All calculations were performed with tabun-conjugated serine (SUN) moiety derived from tabun-inhibited acetylcholinesterase. The B3LYP/6-31+G* calculated free energy surface diagrams and optimized geometries for O-dealkylation process are given in Figs. 1 and 2, respectively. The O-dealkylation process of SUN molecule proceeds via a single-step S_N2 type mechanism involves attack

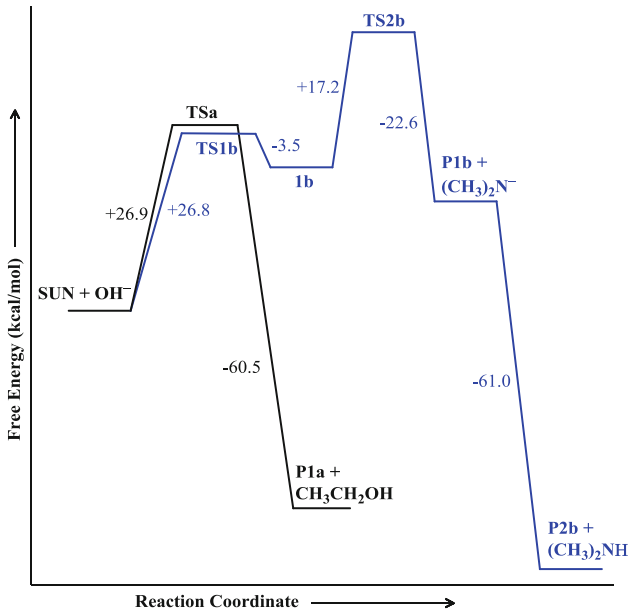

Fig. 1 B3LYP/6-31+G* calculated free energy diagrams for the O-dealkylation (*black line*) and the deamination (*blue line*) process of tabun-conjugated serine (SUN) molecule in aqueous phase

of OH^- ion on the C–O carbon of ethoxy substituent. The hydroxyl nucleophile is produced through activated water molecule [29]. The B3LYP/6-31+G* calculated free energy of activation was found to be 26.9 kcal/mol, which proceeds through the transition state **TSa** (Fig. 1). The calculated $C–O_{(hydroxy)}$ and $C–O_{(ethoxy)}$ bond distances are 2.213 and 1.867 Å, respectively (Fig. 2). The transition-state **TSa** leads to the products **P1a** and ethanol, which is 33.6 kcal/mol more stable than separated reactants (Fig. 1). The overall reaction process is exergonic in nature.

Mass spectrometry (MS) analysis of aged products of tabun-inhibited *h*AChE and first crystallographic study of *m*AChE suggested the deamination process of SUN molecule, which has also been explored [24, 26, 27]. It has been speculated that deamination proceeds through a nucleophilic substitution on the phosphorus atom and the formation of a pentacoordinated trigonal–bipyramidal intermediate [46]. Generally, the most favorable substitution corresponds to the nucleophile approaching the phosphorus atom from the opposite face of the leaving group and thus occupying the apical position. The bonds between apical atoms and the phosphorus atom are relatively longer and weaker than the corresponding equatorial atoms. Therefore, the departure of the leaving group would be more favorable at the apical position [47]. In the deamination process, hydroxide ion attacks to the phosphorus center of SUN molecule opposite to dimethylamine group and leads to the trigonal–bipyramidal intermediate with hydroxide and dimethylamine group at apical positions. The calculated free energy surface and the optimized geometries for deamination process are given in Figs. 1 and 3, respectively. The formation of trigonal–bipyramidal intermediate **1b** proceeds via **TS1b** transition state with activation free energy of 26.8 kcal/mol in the aqueous phase at B3LYP/6-31+G* level of theory (Fig. 1). The calculated P–O bond distances in **TS1b** and **1b** are 2.146 and 1.804 Å, respectively (Fig. 3). The complex formed between the reactants **SUN** and $\mathbf{OH^-}$ was found to be higher in energy than separated reactants in the aqueous phase (Fig. S1, Supporting Information), which suggests that the deamination process is not expected to be influenced by the complex $[\mathbf{SUN–OH}]^-$. The trigonal–bipyramidal intermediate **1b** yields the aged product through the second transition state **TS2b** (Fig. 1). The calculated free energy of activation for **TS2b** is 40.5 kcal/mol with respect to separated reactants. The calculated P–N bond distances in **1b** and **TS2b** are 1.821 and 2.703 Å, respectively. It seems that free energy barrier for **TS2b** is much higher than first transition state **TS1b**, which suggests that the P–N bond breaking process is the rate-determining step for the deamination pathway. The formation of product **P1b** is endergonic in nature by 17.9 kcal/mol (Fig. 1). This endothermicity presumably arises due to the formation of

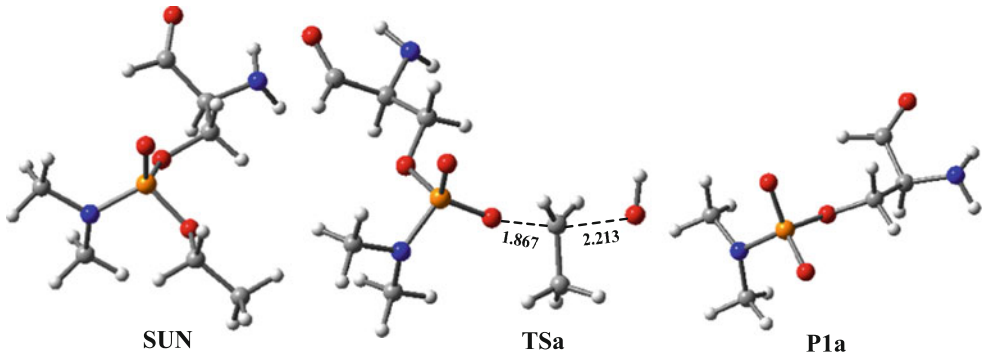

Fig. 2 B3LYP/6-31+G* optimized geometries and selected bond distances (Å) for species involved in the O-dealkylation process of tabun-conjugated serine (SUN) molecule in aqueous phase. (*red* oxygen, *blue* nitrogen, *white* hydrogen, *yellow* phosphorus, *gray* carbon)

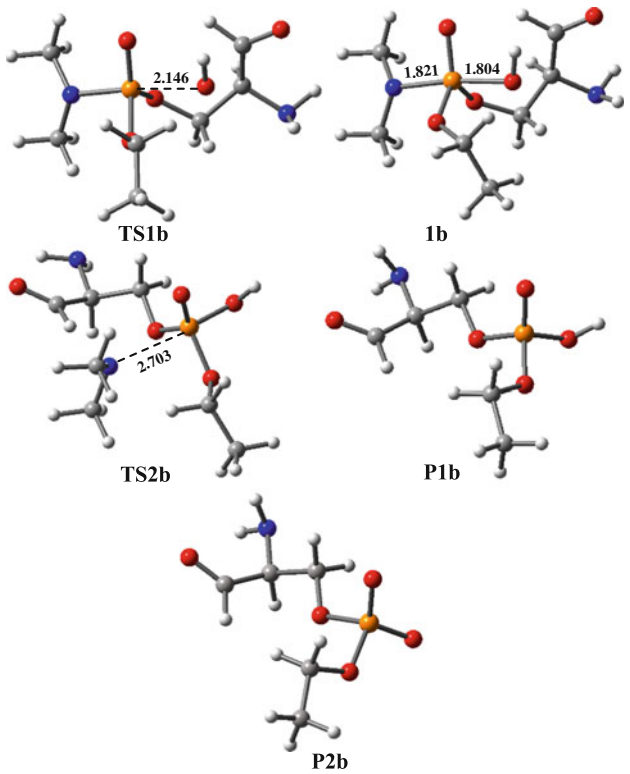

Fig. 3 B3LYP/6-31+G* optimized geometries and selected bond distances (Å) for species involved in the deamination process of tabun-conjugated serine (SUN) molecule in aqueous phase. (*red* oxygen, *blue* nitrogen, *white* hydrogen, *yellow* phosphorus, *gray* carbon)

dimethylamine anion, which might not be the case in the buffered environment of the enzyme. Presumably in the full enzymatic system, the product can possibly rearrange to **P2b + $(CH_3)_2NH$**, which is 61.0 kcal/mol stable than **P1b + $(CH_3)_2N^-$** (Figs. 1, 3). We have shown that the incorporation of imidazole moiety can further facilitate the overall process to be exergonic in nature (vide infra). The calculated free energy profiles for O-dealkylation and deamination processes suggest that the former process is kinetically more favorable. This observation corroborates the crystallographic studies [28, 30].

Recently, on the basis of X-ray crystallographic study, Nachon et al. [31] have reported that the *h*BChE conjugated with *N*-mono methyl analogue of tabun (TA4) is crowded opposite to methylamino group and suggest the attack of water molecule from one of the open faces, adjacent to the methylamino substituents. They have also indicated that the water molecule can approach opposite to the ethoxy group, as this face is more open, and the approaching molecule can be stabilized by hydrogen bonding to Glu197 and activated by His438 [31]. This attack is expected to lead to the formation of trigonal–bipyramidal intermediate with ethoxy and hydroxyl group at apical positions. The proposed deamination process can be facile, if the dimethylamine group moves from its original equatorial to apical position in the rearrangement process (Scheme 1).

We have also explored the rearrangement deamination mechanism for tabun-inhibited serine, which, however, is not reported experimentally as a probable pathway for the aging in this case. The B3LYP/6-31+G* calculated free energy profile and calculated optimized geometries are shown in Figs. 4 and 5, respectively. The calculated free energy of activation for the attack of OH^- ion on the phosphorus center opposite to ethoxy substituent as suggested by Nachon et al. is 26.3 kcal/mol (**TS1c),** which leads to the formation of trigonal–bipyramidal intermediate **1c** with hydroxide and ethoxy groups at apical position (Figs. 4, 5). Trigonal–bipyramidal intermediate **1c** undergoes a rearrangement process through the transition state **TS2c** and gives another trigonal–bipyramidal intermediate **2c** with dimethylamine group at the apical position. This rearrangement process proceeds with activation free energy of 7.5 kcal/mol with respect to **1c** (Fig. 4). The calculated bond angles for O–P–$O_{(hydroxy)}$ are 92.4° and 124.5°, and for O–P–$O_{(ethoxy)}$ are 95.8° and 121.8° for **1c** and **2c**, respectively, suggesting the progression of movement of

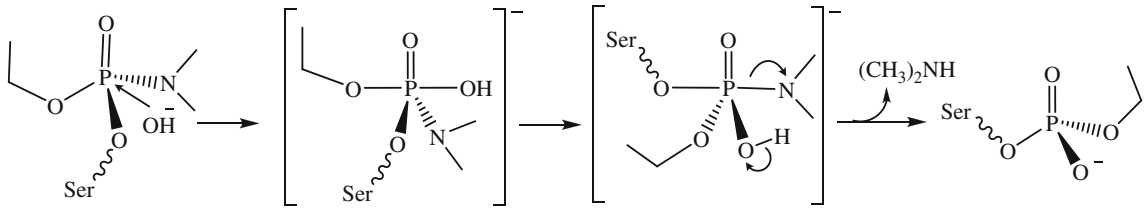

Scheme 1 Proposed deamination pathway of tabun-conjugated serine (SUN) molecule involved rearrangement of intermediate

ethoxy and hydroxyl groups from apical to equatorial positions. Finally, the P–N bond breaking process proceeds through the transition state **TS3c** with 22.1 kcal/mol free energy of activation. This free energy diagram indicates that the attack of OH^- on the phosphorus center of SUN is the rate-determining step, and the deamination products formation is exergonic in nature (Fig. 4). The calculated results show that the deamination pathway proposed by Nachon et al. is energetically more facile compared to the other deamination process. These results suggest that the O-dealkylation process and deamination process involving rearrangement mechanism can compete for the aging of tabun-inhibited AChE (Figs. 1, 4). According to the proposed mechanism, the His447 imidazolium participates in the O-dealkylation process via stabilizing the negative charge on the polarized C–O oxygen of ethoxy substituent [28]. Therefore, we have decided to explore the role of His447 in the aging process of the tabun-inhibited AChE. Additional calculations were performed with SUN molecule interacted with imidazole ring of His447 residue (**1**) (Fig. 6). The calculated activation free energy for O-dealkylation process is 23.9 kcal/mol, which is 3.0 kcal/mol less than activation free energy calculated without imidazole ring (Figs. 1,7). This clearly supports the influence of His447 during O-dealkylation process. The imidazole ring was found to be hydrogen bonded with the $O_{(ethoxy)}$ atom during the process (Fig. 8). The N–H···O distance in transition state **1-TSa** is 1.851 Å, which further decreases to 1.745 Å in product **1-P1a**.

In the deamination process, the activation free energy for hydroxide ion attack on phosphorus center is 22.7 kcal/mol, which is 4.1 kcal/mol less than barrier calculated without imidazole ring (Figs. 1, 7). The lowering in free energy barrier is observed due to hydrogen bonding of the nitrogen of dimethylamine group with the imidazole ring. The movement of the imidazole ring was noticed during the optimization of transition state **1-TS1b** from ethoxy oxygen to nitrogen of dimethylamine group (Fig. 9). This process shows that the P–N bond breaking is exergonic in nature with the involvement of the imidazole ring (Fig. 7). Interestingly, the imidazole ring transfers the proton to the leaving dimethylamine group in the P–N bond breaking process. The trigonal–bipyramidal intermediate **1-I1b** proceeds to another intermediate **1-I2b** through barrier less

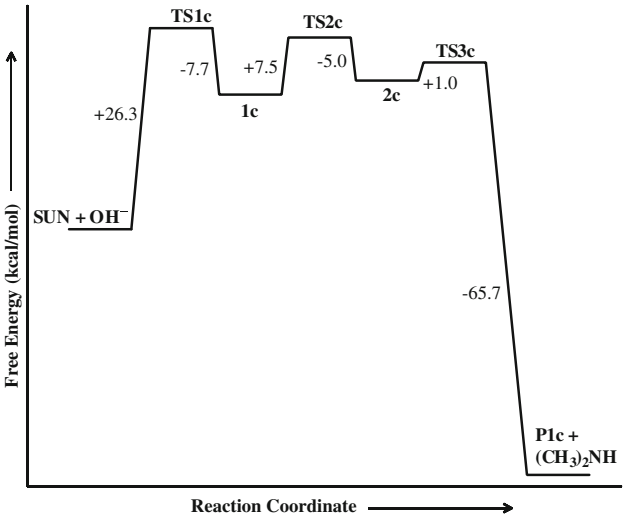

Fig. 4 B3LYP/6-31+G* calculated free energy diagram for deamination process of tabun-conjugated serine (SUN) molecule in aqueous phase involved rearrangement of trigonal–bipyramidal intermediate

hydrogen transfer transition state **1-TS2b** (Fig. 7). The free energy of activation for the proton transfer was found to be -0.9 kcal/mol; however, the electronic energy of activation in the solvated state was 1.1 kcal/mol (Fig. S2, Supporting Information). The product **1-P1b** is 24.6 kcal/mol more stable than reactants. The product **1-P1b** is most likely to be formed in this isolated system, while in the full enzymatic system, the product can possibly rearrange to the proper protonation state **1-P2b** presumably through the participation of solvent molecules. This can lead to the more stabilized product (**1-P2b**) by 22.8 kcal/mol than that of **1-P1b** (Figs. 7,9).

The calculated free energy surface with imidazole ring for deamination mechanism proposed by Nachon et al. is similar to the free energy surface calculated without imidazole ring (Figs. 4, 7). However, the calculated free energy barrier for rate-determining step is 5.3 kcal/mol lower than the barrier obtained in the absence of imidazole ring (Figs. 4, 7). The calculated geometries are given in Fig. 10. The DFT calculated results show that the O-dealkylation and the deamination processes are largely comparable for the aging of tabun-inhibited AChE with slight preference toward the rearrangement mechanism (Fig. 7).

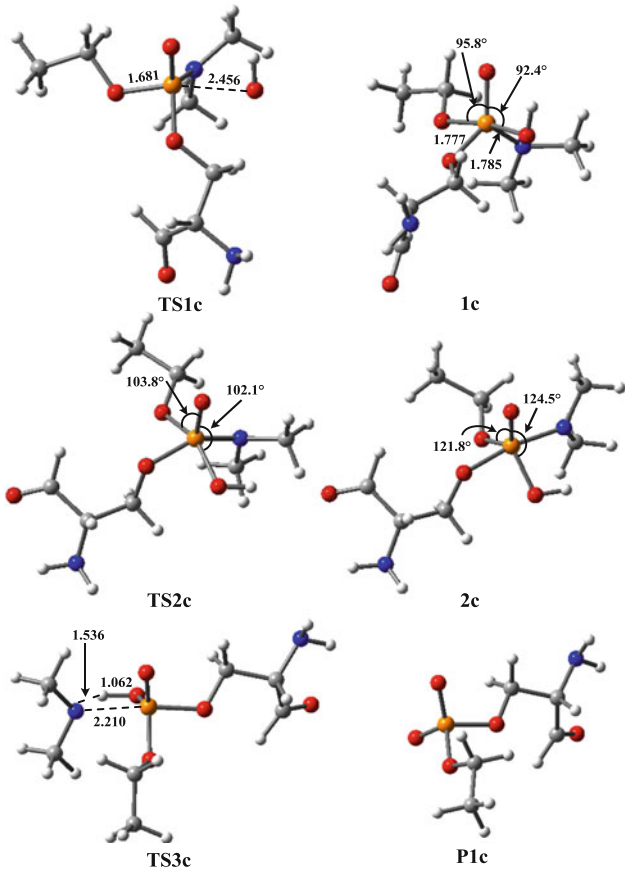

Fig. 5 B3LYP/6-31+G* optimized geometries, selected bond distances (Å), and bond angles (°) for species involved in the deamination processes of tabun-conjugated serine (SUN) molecule in aqueous phase involved rearrangement of trigonal–bipyramidal intermediate. (*red* oxygen, *blue* nitrogen, *white* hydrogen, *yellow* phosphorus, *gray* carbon)

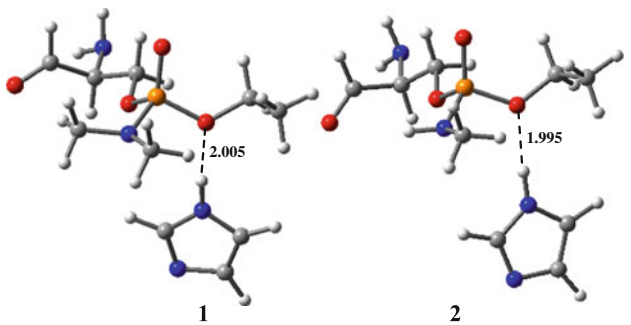

Fig. 6 B3LYP/6-31+G* optimized geometries and O···H distances (Å) for tabun-inhibited serine with imidazole ring (**1**) and TA4-inhibited serine with imidazole ring (**2**) in aqueous phase. (*red* oxygen, *blue* nitrogen, *white* hydrogen, *yellow* phosphorus, *gray* carbon)

The importance of deamination process involving rearrangement of TBP intermediate was obtained with the *N*-mono methyl analogue of tabun (TA4) [31]. Therefore, we have examined the competing aging processes of TA4-inhibited serine **2,** with B3LYP/6-31+G* level of theory

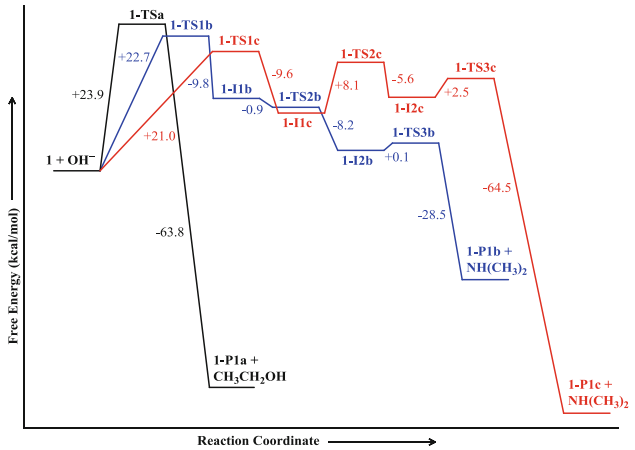

Fig. 7 B3LYP/6-31+G* calculated free energy diagrams for the O-dealkylation (*black line*) and deamination (*blue line*) processes of tabun-conjugated serine molecule (**1**) in aqueous phase. Free energy diagram for deamination process that involved rearrangement of trigonal–bipyramidal intermediate is also given (*red line*)

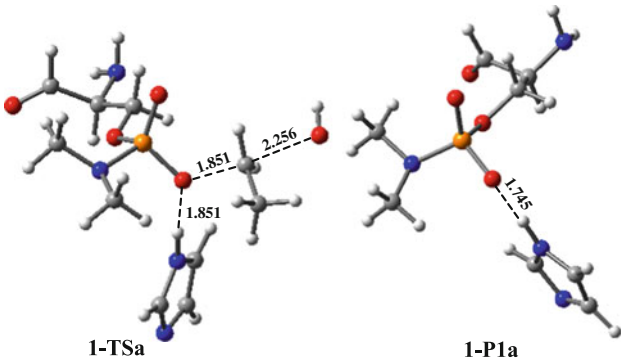

Fig. 8 B3LYP/6-31+G* optimized geometries and selected bond distances (Å) for species involved in the O-dealkylation processes of tabun-conjugated serine molecule (**1**) in aqueous phase. (*red* oxygen, *blue* nitrogen, *white* hydrogen, *yellow* phosphorus, *gray* carbon)

(Fig. 6). The calculated free energy diagrams for the O-dealkylation and deamination processes for TA4-inhibited serine (**2**) are almost similar to that of tabun-inhibited serine (**1**) (Figs. 7, 11). In the deamination profile, two transition states **2-TS2b** and **2-TS3b** have small negative free energy barrier; however, they have positive electronic energy barriers and connected through IRC (Fig. S3 Supporting Information). However, the calculations performed for the deamination process of **2** via rearrangement mechanism as proposed by Nachon et al., showed that the free energy of activation for hydroxide ion attack on phosphorus center is much lower compared to the tabun-inhibited serine (**1**). The lowering in free energy of activation in this case arises due to the intermolecular hydrogen bonding between the amine hydrogen of **2** and the hydroxide ion in transition state **2-TS1c** (Fig. S4c, Supporting Information). Further, note that the hydrogen bonding can also be formed between **2** and OH^- ion in the

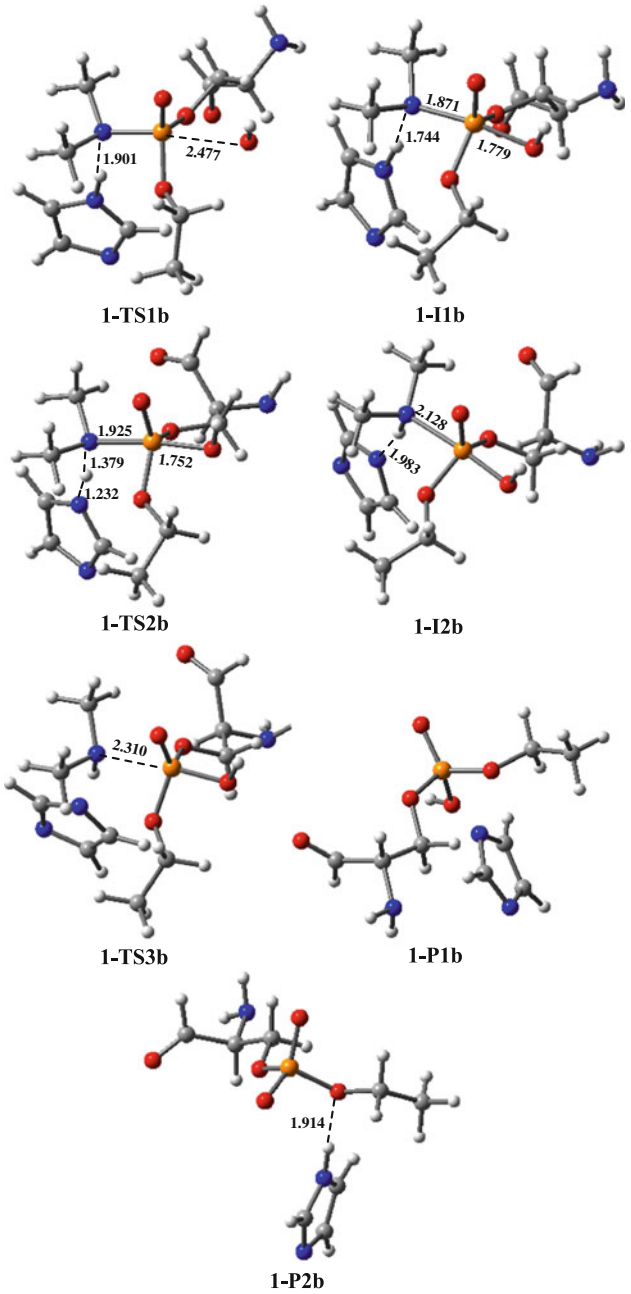

Fig. 9 B3LYP/6-31+G* optimized geometries and selected bond distances (Å) for species involved in the deamination processes of tabun-conjugated serine molecule (**1**) in aqueous phase. (*red* oxygen, *blue* nitrogen, *white* hydrogen, *yellow* phosphorus, *gray* carbon)

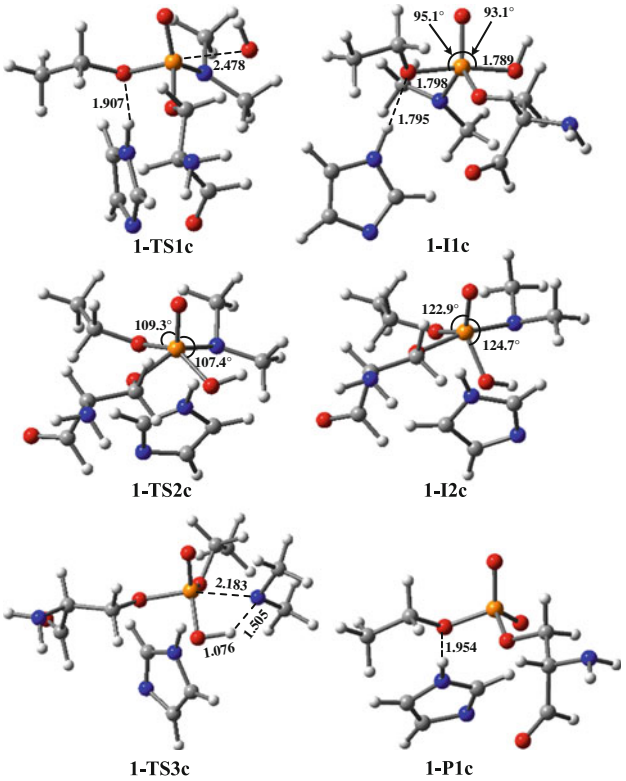

Fig. 10 B3LYP/6-31+G* optimized geometries, selected bond distances (Å), and bond angles (°) for species involved in the deamination processes of tabun-conjugated serine molecule (**1**) in aqueous phase involved rearrangement of trigonal–bipyramidal intermediate. (*red* oxygen, *blue* nitrogen, *white* hydrogen, *yellow* phosphorus, *gray* carbon)

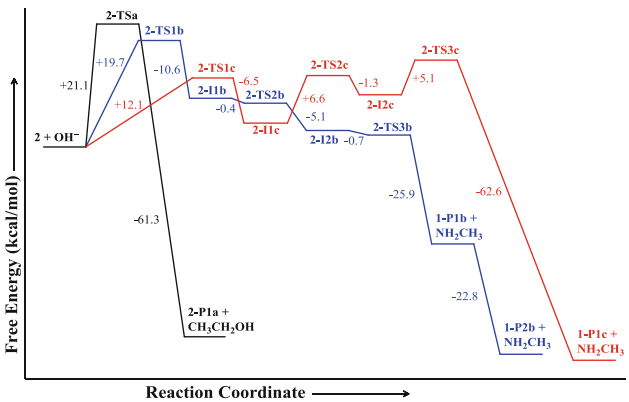

Fig. 11 B3LYP/6-31+G* calculated free energy diagrams for the O-dealkylation (*black line*) and deamination (*blue line*) process of TA4-conjugated serine molecule (**2**) in aqueous phase. Free energy diagram for deamination process that involved rearrangement of trigonal–bipyramidal intermediate is also given (*red line*)

form of a complex, as observed in the transition state. Therefore, additional calculations have been performed to obtain the complex **[2 + OH$^-$]**, which is 5.3 kcal/mol more stable than the respective isolated reactants. The calculated activation barrier for **2-TS1c** with respect to the complex **[2 + OH$^-$]** is 17.4 kcal/mol, which is still lower than corresponding activation barrier calculated for tabun-inhibited serine **1**. Such a lower energy complex was not observed in the case of **1** with OH^- ion (Fig. S5, Supporting Information). In the case of **2,** the P–N bond breaking step is the rate determining in the free energy surface diagram with the activation free energy of 16.0 kcal/mol to separated reactants. The overall free

energy surface suggests a clear preference for the deamination process via rearrangement mechanism for **2**, which supports the crystal study [31].

In addition to calculations with IEF-PCM solvation model, calculations were also performed using SMD solvation model [43]. SMD is a universal solvation model, where "universal" denotes its applicability to any charged or uncharged solute in any solvent medium for which a few key descriptors are known (in particular, dielectric constant, refractive index, bulk surface tension, and acidity and basicity parameters) [43]. This model is recommended for absolute solvation energies and other properties for which the non-electrostatic terms are significant [43]. Full optimizations were performed for all studied mechanisms of the aging process of tabun-inhibited and TA4-inhibited serine. The calculated free energy barriers with SMD solvation model are higher than free energy barriers calculated with IEF-PCM solvation model. Overall, the predictions delivered using SMD solvation model seem to be similar to that of IEF-PCM solvation model for the aging processes of SUN and TA4-inhibited serine (Figs. S6, S7, S8, and S9, Supporting Information).

4 Conclusions

In this work, we have carried out the mechanism of the aging process of tabun-conjugated AChE and its analogue TA4 with DFT B3LYP/6-31+G* calculations. The O-dealkylation (C–O bond breaking) and deamination (P–N bond breaking) pathways have been examined as suggested by mass and crystallographic studies. O-dealkylation process has been predicted to be a one step S_N2 type mechanism, whereas the deamination process proceeds via two steps addition–elimination reaction at the phosphorus center of SUN molecule. Further, the recently proposed deamination mechanism by Nachon et al. has also been examined with the tabun-conjugated AChE. This deamination mechanism of aging of tabun-conjugated AChE involves the rearrangement of the TBP intermediate. The rearrangement of TBP intermediate involves the movement of dimethylamine group from equatorial to apical position. The model study performed with tabun-conjugated AChE showed that the O-dealkylation and deamination involving the rearrangement processes are largely comparable in this case. The incorporation of imidazole group of catalytic residue His447 showed marked decrease in the free energies of activation for all the studied reaction pathways. The calculations performed with both IEF-PCM and SMD solvation models suggest that O-dealkylation and deamination processes are rather comparable in nature in the case of tabun-inhibited serine. Full dynamical study with complete enzymatic environment may shed some more light in the aging process of tabun-inhibited AChE. However, in the case of *N*-mono methyl tabun analogue, TA4 showed that the deamination with the rearrangement process is markedly preferred, which supports the Nachon et al. [31] proposal based on the crystallographic studies. This study infers that the analogues considered for the aging process may not always correlate well with the real substrates.

Acknowledgments Authors thank DST, New Delhi, India, and DAE–BRNS, Mumbai, India, for financial support of this work. MKK is thankful to UGC, New Delhi, India, for awarding fellowship. We thank the reviewers for their comments and suggestions that have helped us to improve the paper.

References

1. Sussman JL, Harel M, Frolow F, Oefner C, Goldman A, Toker L, Silman I (1991) Science 253:872–879
2. Taylor P, Lappi S (1975) Biochemistry 14:1989–1997
3. Harel M, Schalk I, Ehret-Sabatier L, Bouet F, Goeldner M, Hirth C, Axelsen PH, Silman I, Sussman JL (1993) Proc Natl Acad Sci USA 90:9031–9035
4. Quinn DM (1987) Chem Rev 87:955–979
5. Massoulié J, Pezzementi L, Bon S, Krejci E, Vallette FM (1993) Prog Neurobiol 41:31–91
6. Patočka J, Kuča K, Jun D (2004) Acta Medica 47:215–230
7. Wang J, Roszak S, Gu J, Leszczynski J (2005) J Phys Chem B 109:1006–1014
8. Wang J, Gu J, Leszczynski J (2006) J Phys Chem B 110:7567–7573
9. Järv J (1984) Bioorg Chem 12:259–278
10. Taylor P, Radic Z, Hosca NA, Camp S, Marchot P, Berman HA (1995) Toxicol Lett 82–83:453–458
11. Bismuth C, Inns RH, Marrs TC (1992) Efficacy, toxicity and clinical use of oximes in anticholinesterase poisoning. In: Ballantyne B, Marrs TC (eds) Clinical and experimental toxicology of organophosphates and carbamates. Butterworth & Heinemann, Oxford, pp 555–577
12. Patočka J, Cabal J, Kuča K, Jun D (2005) J Appl Biomed 3:91–99
13. Kovach IM, Bennet AJ, Bibbs JA, Zhao Q (1993) J Am Chem Soc 115:5138–5144
14. Benschop HP, de Jong LPA (2001) Toxicokinetics of nerve agents. In: Somani SM, Romano JA (eds) Chemical warfare agents: toxicity at low levels. CRC Press, Boca Raton, pp 25–81
15. Baggot JD (1994) Am J Vet Res 55:689–691
16. Clement JG, Erhardt N (1994) Arch Toxicol 68:648–655
17. Worek F, Reiter G, Eyer P, Szinicz L (2002) Arch Toxicol 76:523–529
18. Worek F, Thiermann H, Szinicz L, Eyer P (2004) Biochem Pharmocol 68:2237–2248
19. Millard CB, Kryger G, Ordentlich A, Greenblatt HM, Harel M, Raves ML, Segall Y, Barak D, Shafferman A, Silman I, Sussman JL (1999) Biochemistry 38:7032–7039
20. Segall Y, Waysbort D, Barak D, Ariel N, Doctor BP, Grunwald J, Ashani Y (1993) Biochemistry 32:13441–13450
21. Saxena A, Viragh C, Frazier DS, Kovach IM, Maxwell DM, Lockridge O, Doctor BP (1998) Biochemistry 37:15086–15096
22. Heilbronn E (1963) Biochem Pharmacol 12:25–36
23. Carletti E, Aurbek N, Gillon E, Loiodice M, Nicolet Y, Fontecilla-Camps JC, Masson P, Thiermann H, Nachon F, Worek F (2009) Biochem J 421:97–106

24. Ekström F, Akfur C, Tunemalm A-K, Lundberg S (2006) Biochemistry 45:74–81
25. Ekström F, Pang YP, Boman M, Artursson E, Akfur C, Börjegren S (2006) Biochim Pharmacol 72:597–607
26. Barak D, Ordentlich A, Kaplan D, Barak R, Mizrahi D, Kronman C, Segall Y, Velan B, Shafferman A (2000) Biochemistry 39:1156–1161
27. Elhanany E, Ordentlich A, Dgany O, Kaplan D, Segall Y, Barak R, Velan B, Shafferman A (2001) Chem Res Toxicol 14:912–918
28. Carletti E, Li H, Li B, Ekström F, Nicolet Y, Loiodice M, Gillon E, Froment MT, Lockridge O, Schopfer LM, Masson P, Nachon F (2008) J Am Chem Soc 130:16011–16020
29. Nachon F, Asojo OA, Borgsthal GEO, Masson P, Lockridge O (2005) Biochemistry 44:1154–1162
30. Carletti E, Colletier J-P, Dupeux F, Trovaslet M, Masson P, Nachon F (2010) J Med Chem 53:4002–4008
31. Nachon F, Carletti E, Worek F, Masson P (2010) Chem Biol Interact 187:44–48
32. Ekström FJ, Åstot C, Pang Y-P (2007) Clin Pharmacol Ther 82:282–293
33. Becke AD (1993) J Chem Phys 98:5648–5652
34. Lee C, Yang W, Parr RG (1988) Phys Rev B 37:785–789
35. Beck JM, Hadad CM (2008) Chem Biol Interact 175:200–203
36. Hehre WJ, Radom L, Schleyer PvR, Pople JA (1988) Ab initio molecular orbital theory. Wiley, New York
37. Frisch MJ, Trucks GW, Schlegel HB, Scuseria GE, Robb MA, Cheeseman JR, Scalmani G, Barone V, Mennucci B, Petersson GA, Nakatsuji H, Caricato M, Li X, Hratchian HP, Izmaylov AF, Bloino J, Zheng G, Sonnenberg JL, Hada M, Ehara M, Toyota K, Fukuda R, Hasegawa J, Ishida M, Nakajima T, Honda Y, Kitao O, Nakai H, Vreven T, Montgomery, Jr JA, Peralta JE, Ogliaro F, Bearpark M, Heyd JJ, Brothers E, Kudin KN, Staroverov VN, Keith T, Kobayashi R, Normand J, Raghavachari K, Rendell A, Burant JC, Iyengar SS, Tomasi J, Cossi M, Rega N, Millam JM, Klene M, Knox JE, Cross JB, Bakken V, Adamo C, Jaramillo J, Gomperts R, Stratmann RE, Yazyev O, Austin AJ, Cammi R, Pomelli C, Ochterski JW, Martin RL, Morokuma K, Zakrzewski VG, Voth GA, Salvador P, Dannenberg JJ, Dapprich S, Daniels AD, Farkas O, Foresman JB, Ortiz JV, Cioslowski J, Fox DJ (2010) Gaussian 09, Revision B01. Gaussian, Inc, Wallingford, CT
38. Cancès E, Mennucci B, Tomasi JJ (1997) Chem Phys 107:3032–3041
39. Mennucci B, Tomasi JJ (1997) Chem Phys 106:5151–5158
40. Barone V, Cossi M, Tomasi J (1997) J Chem Phys 107:3210–3221
41. Barone V, Cossi M, Tomasi J (1998) J Comput Chem 19:404–417
42. Tomasi J, Mennucci B, Cancès E (1999) J Mol Struct (Theochem) 464:211–226
43. Marenich AV, Cramer CJ, Truhlar DG (2009) J Phys Chem B 113:6378–6396
44. González C, Schlegel HB (1990) J Phys Chem 94:5523–5527
45. González C, Schlegel HB (1991) J Chem Phys 95:5853–5860
46. Hörnberg A, Tunemalm A-K, Ekström F (2007) Biochemistry 46:4815–4825
47. Thatcher GRJ, Kluger R (1989) Adv Phys Org Chem 25:99–265